DNS OF TURBULENT IMPINGING JETS ON ROUGH SURFACES USING A PARAMETRIC FORCING APPROACH

F. Secchi, D. Gatti and B. Frohnapfel

Institute of Fluid Mechanics (ISTM), Karlsruhe Institute of Technology (KIT)

francesco.secchi@kit.edu

Abstract

This work presents direct numerical simulations (DNS) of a circular turbulent jet impinging on rough plates. A parametric forcing approach (PFA) accounts for surface roughness effects by applying a forcing term into the Navier-Stokes equations within a thin layer in the near-wall region. The application of the PFA in the context of spatially developing flows is the essential aspect of the investigation. The method is known to produce accurate predictions of the velocity field in fully developed turbulent flows while avoiding the demanding grid resolution required by an immersed boundary method (IBM) approach. The comparison between PFA results and IBM-resolved roughness DNS allows addressing the advantages and limitations of the PFA in the context of spatially developing flows.

1 Introduction

Technical fluid flows occur over surfaces that are rough as a result, for instance, of the manufacturing process or wear. From the fluid-dynamics perspective, a wall is considered either rough or smooth according to the flow characteristics. For wall-bounded turbulent flows, the interaction of the smallest scales of motion with roughness elements usually results in enhanced wall-friction and heat exchange coefficients with respect to a comparable flow over a smooth wall. Despite the constantly increasing computational power, investigating the effects of roughness via fully-resolved numerical simulations of turbulent flows over rough walls remain a challenging task. In this context, immersed boundary methods (IBM) have become standard practice for simulating complex boundaries in DNS. Despite their versatility, IBM require heavy mesh refinement when complex geometries are involved. Resolving roughness geometries within Cartesian grids may exceed the grid resolution requirements demanded to capture the smallest eddies in the flow. The parametric forcing approach (PFA) introduced by Busse and Sandham (2012) appears as a promising alternative. Similarly to IBM, no body-conform mesh is required to describe the roughness. The PFA adds a forcing term into the Navier-Stokes equation in a thin layer where surface roughness is present. The added unit volume force serves to account for the form drag induced by roughness elements. The modified PFA presented by Forooghi et al. (2018a) includes an additional viscous drag contribution to the original formulation. The same work shows the successful application of the method for predicting the flow characteristics of fully developed turbulent channel flows with rough walls. The present research aims to employ the PFA into the DNS of turbulent axisymmetric jets impinging on rough plates. After jet impingement, the flow occurring next to the impingement plate is a spatially developing flow. Such flow configuration represents a scenario in which the PFA has not been tested so far.

2 Methodology

Flow configuration

Figure (1) depicts a sketch of the flow configuration. The jet originates from a fully developed turbulent pipe flow and impinges on a plate placed $2D$ away from the jet exit section (D represents the pipe diameter). The Reynolds number is $Re = 10000$ (Re is based on the pipe diameter and the bulk mean velocity in the pipe). The flow is incompressible and free from volume forces, except in the near-wall region where a distributed forcing is applied to introduce the effects of surface roughness into the flow. Fully developed inflow boundary conditions are enforced at the inlet section of the computational domain using a periodic precursor simulation of a fully developed turbulent pipe flow.
The flow solver employed is `Nek5000` developed by Fisher et al. (2008-2020). It is an open-source code based on the spectral element method of Maday and Patera (1989). `Nek5000` is well known for its efficient parallel scaling characteristics and for retaining high order spectral accuracy in the solution.

Parametric forcing approach

The approach followed in the present work is equivalent to the "modified PFA" introduced by Forooghi et al. (2018a). A forcing term f_i is introduced into the momentum equation of the incompress-

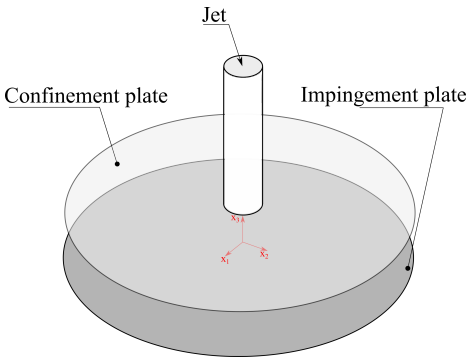

Figure 1: Impinging jet flow configuration used in the simulations.

ible Navier-Stokes equations:

$$\frac{\partial u_j}{\partial x_j} = 0 \tag{1}$$

$$\frac{\partial u_i}{\partial t} + u_j \frac{u_i}{\partial x_j} = -\frac{\partial p}{\partial x_i} + \frac{1}{Re}\frac{\partial^2 u_i}{\partial x_j x_j} + f_i \tag{2}$$

The above equations are valid for $(i, j = 1,\ 2,\ 3)$ and summation over repeated indexes is implied. Equations (1) and (2) are made dimensionless using the mean bulk velocity in the pipe and the pipe diameter D. Therefore, the Reynolds number appearing in equation (2) is defined as $Re = U_b D/\nu$, where ν indicates the kinematic viscosity of the fluid. Within the present formulation, forcing is applied only in the wall-parallel directions $x_1 - x_2$, therefore $f_3 = 0$. Furthermore, it is assumed that the volume force f_i is made up of a linear (with the local fluid velocity) and a quadratic term. The former represents the viscous drag contribution of roughness elements, while the latter accounts for their form drag. By introducing two shape functions A and B, the volume force can thus be expressed as:

$$f_i = -A(x_3)u_i - B(x_3)u_i|u_i| \tag{3}$$

The functional dependency of the functions A and B on the wall-normal direction x_3 only is specific for the present case and will be clarified in the following of this section. The analogy with the Darcy-Brinckmann-Forchheimer equation in the context of flow through porous media is evident in equation (3) (see, for instance, Vafai and Kim (1995)). Furthermore, the similarity with modeling of flow through porous media is additionally exploited to determine the function A appearing in equation (3). As derived in Forooghi et al. (2018a), A is expressed as:

$$A^* = \frac{\nu^*}{K^*} \tag{4}$$

where ν^* is the viscosity of the fluid, while K^* is the permeability of the porous medium (asterisks in equation (4) denote dimensional quantities). Different approaches can be followed in order to relate the permeability K to the geometrical features of the porous medium or, in this case by analogy, of the rough wall geometry. One possibility, as suggested by Forooghi et al. (2018a), is to use the Kozney-Carman theory and, hence, the similarity between flow through porous media and flow through bundles of capillary conduits (the Kozney-Carman theory is explained, for example, in Kaviany (2012)). By following this approach, the proper non-dimensional form of the function A is found to be:

$$A(x_3) = \frac{K_k}{Re}\frac{s(x_3)^2}{\epsilon(x_3)^3} \tag{5}$$

In equation (5), K_k is the Kozney constant arising from the adoption of the Kozney-Carman theory, $s(x_3)$ is the total wetted surface area per unit total volume, and $\epsilon(x_3)$ is the porosity. In particular, the porosity is defined as the ratio of the fluid volume to the total volume. Both, the wetted area and the porosity are here considered functions of the wall-normal direction x_3 because the surface roughness is modelled homogeneously in the x_1 and x_2 directions.

By recalling the physical meaning of the quadratic term in equation 3, it is straightforward to identify the shape function B using the analogy with the form drag induced by a bluff body. This results in:

$$B(x_3) = \frac{1}{2}C_d s_f(x_3)^2 \tag{6}$$

where C_d is interpreted as the drag coefficient, and $s_f(x_3)$ is the total frontal projected area (averaged in the x_1 and x_2 directions) of the roughness per unit total volume.

From equations (5) and (6), it is observed that the shape of the two functions A and B is completely determined by the geometric characteristics of the roughness. The constants K_k and C_d appearing in the definition of the volume force f_i can be used to tune the model. In this respect, it is remarked that the model constants could be also related to the features of the rough surface in order to have a fully predetermined model which does not necessitate any *ad-hoc* tuning. However, a clear connection between these constants and geometrical features of the surface roughness is not yet available and, for this reason, the constants are considered as free parameters in this work.

Immersed boundary method

Reference DNS are obtained by using the IBM of Goldstein et al. (1993). Similarly to the PFA, this particular IBM introduces a forcing term to the momentum equation. The forcing is applied only for grid points lying within the solid phase of the computational domain, thus a complete description of the solid body geometry can be achieved with the IBM, provided that the grid resolution is sufficiently fine. The forcing term appearing in equation (2) is in this case:

$$f_i = -\alpha \int_0^t (u_i - U_{body,i})\,\mathrm{d}t' - \beta\,(u_i - U_{body,i}) \tag{7}$$

Table 1: Models constants adopted in this study

Method	C_1^*	C_2^*
PFA	200	50
IBM	$2 \cdot 10^5$	200

* The two constants C_1 and C_2 correspond to K_k and C_d in the case of the PFA, whereas to α and β in the case of the IBM.

where α and β are two constants that can be adjusted, and $U_{body,i}$ is the i^{th} component of the prescribed velocity of the solid body. In the present study, only stationary walls are considered, therefore $U_{body,i} = 0$ for $i = 1, 2, 3$. The volume force introduced in equation (7) acts as the input of a proportional integral controller which aims at at keeping the local fluid velocity to the prescribed value $\mathbf{U_{body}}$ (thus, in the considered case, $\mathbf{U_{body}} = 0$

Models constants

As it is clear from the preceding discussion, both the PFA and the adopted IBM require to set two constant parameters. Regarding the IBM, this topic is well covered in the original work of Goldstein et al. (1993) where it is shown that the order of magnitude of α and β needs to be properly adjusted for each considered flow configuration, but the actual value of the two constants is irrelevant on the final result. On the assumption that the response of the system to an input force as that in equation (7) can be approximated by the response of a linear system, the parameters α and β assume a clear significance. In particular, the integral constant α determines the natural frequency of the system, while the proportional constant β is related to the damping ratio. Hence, large values of α allow to track fast fluctuations of the local fluid velocity, while large values of β help to damp out oscillations. Clearly, the major limitation encountered when setting the two parameters is the numerical stability of the time marching technique adopted. Similar reasoning can be performed also for the parameters K_k and C_d of the PFA, but no clear meaning can be attached to the two constants in this case. Since no prior knowledge about the PFA applied to impinging jet configurations is available, model constants used in this study are picked without any modification from turbulent channel flow simulations in which the PFA was successfully applied to account for surface roughness effects. The set of constants adopted for all the presented cases are reported in table 1.

Surface roughness

Rough surfaces consist of wall-height distributions in the $x_1 - x_2$ plane having prescribed statistical properties. The algorithm employed to design roughness geometries is completely based on the procedure presented in Pèrez-Ràfols and Almqvist (2019). This is an iterative approach which allows to generate roughness topologies having prescribed power spectrum (PS) and probability density function (PDF). By scaling properly the resulting surface height distribution, it is possible to characterize different rough surfaces. In this respect, the main quantity adopted in the present work to distinguish between different rough surfaces is the k_{99} (*i.e.* the 99% confidence interval of the roughness height PDF distribution). Three different rough surfaces are investigated in this study; these are characterized by $k_{99} = 0.05D$, $k_{99} = 0.12D$ and $k_{99} = 0.15D$. A Gaussian PDF is adopted for all the cases, while the PS is prescribed to match the PS of a realistic rough surface as in Forooghi et al. (2018b). The effective slope parameter (ES) (as defined in Napoli et al. (2008)) is kept constant $ES = 0.41$ for the three cases. Samples of the obtained roughness geometries are displayed in figure 2. The $x_3/D = 0$ plane is located at the lowest valley of the roughness height distribution. This is consistent with surface roughness caused by deposition of sediments in real applications.

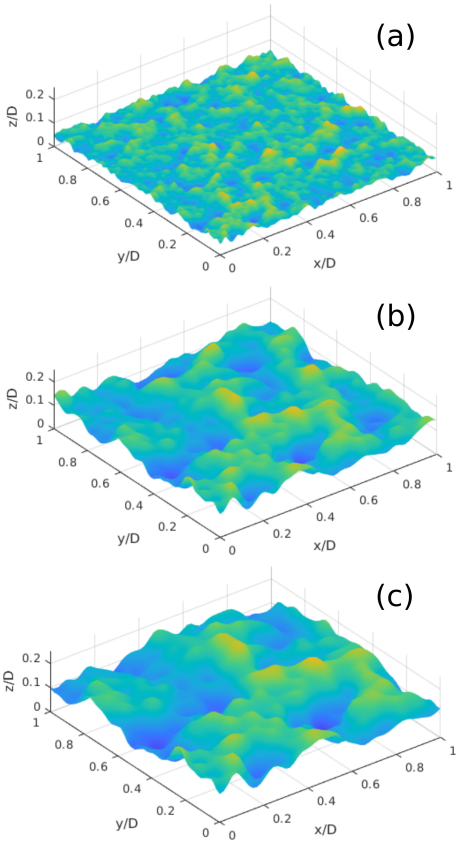

Figure 2: Rough surfaces samples. (a) $k_{99}/D = 0.05$; (b) $k_{99}/D = 0.12$; (c) $k_{99}/D = 0.15$

The three rough surfaces are modelled within the PFA via the two roughness shape functions A and B defined in equations (5) and (6) respectively. The normalized shape functions for the three investigated surfaces are reported in figure 3. From the figure, it is evident that the function A, which tunes the effect of the viscous drag term of the forcing (*i.e.* the linear term), is relevant only over a thin layer very close to

$x_3/D = 0$. On the other hand, the function B has a wider support which spans the entire thickness of the roughness height distribution. It is remarked that the overall contribution of the form drag term of the PFA forcing (*i.e.* the quadratic term) becomes weaker close to the wall where the local fluid velocity tends to zero.

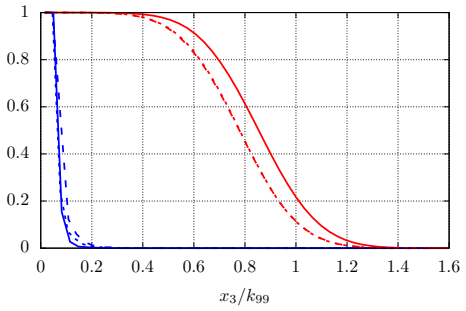

Figure 3: Roughness shape functions. Function A: ——, $k_{99}/D = 0.05$; - - - -, $k_{99}/D = 0.12$; - - - - $k_{99}/D = 0.15$. Function B: ——, $k_{99}/D = 0.05$; - - - -. $k_{99}/D = 0.12$; - - - - $k_{99}/D = 0.15$

3 Results

Flow field statistics are computed by averaging in time (on the fly during the simulations) and in the circumferential direction. Hence, the resulting averaged flow field is two dimensional, with any statistical quantity being a function of the radial distance r from the jet axis and the wall-normal distance x_3. A first comparison is done for the mean radial velocity profiles. After the jet impingement, a radial wall-jet develops along the rough plate where a boundary layer develops and thickens rapidly due to the entrainment of the outer quiescent fluid. Mean radial velocity profiles at different radial locations are depicted in figure 4 for the three rough wall cases. The velocity profiles are plotted using a logarithmic scale for the wall-normal coordinate x_3 to better visualize the near-wall region. In the figure, a black dashed line represents the k_{99} height of the roughness, while blue and red lines represent IBM and PFA resolved results respectively. The velocity profiles shown in the figure correspond to the radial locations $r/D = 0.6,\ 0.8,\ 1.0,\ 1.2,\ 1.4,\ 1.5,\ 2.0$, but they are plotted shifted away from each other of 1.0 units for better visualization. It is observed that PFA resolved profiles display a non-zero velocity at all the locations below the k_{99} roughness height of the considered rough surface. This is in accordance with the PFA as, contrary to the IBM adopted, the applied forcing does not aim at enforcing a zero velocity within the forcing layer. For $x_3/D > k_{99}/D$, a good agreement between the shapes of the radial velocity profiles is observed at all radial locations for all the three cases. In

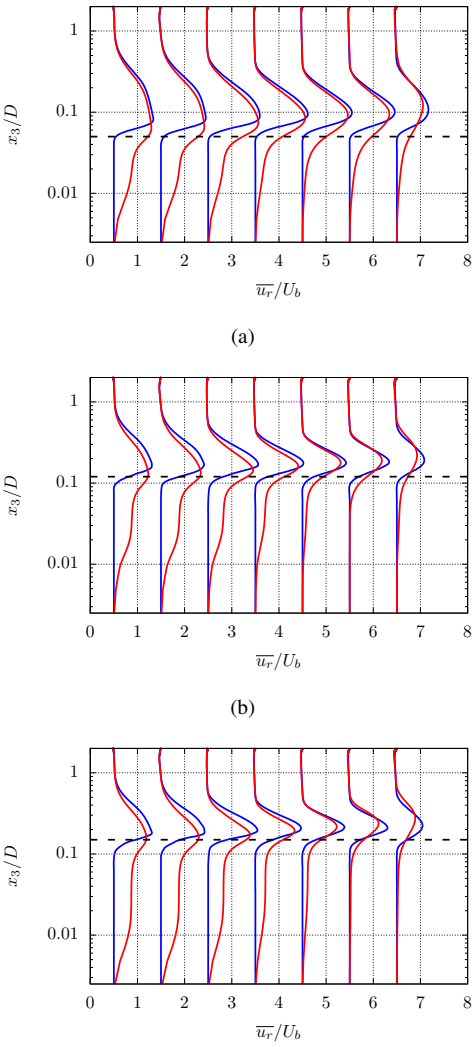

Figure 4: Mean radial velocity profiles at $r/D = 0.6,\ 0.8,\ 1.0,\ 1.2,\ 1.4,\ 1.5,\ 2.0$. Profiles are shifted to the right from each other by 1.0 units for better visualization. ——, IBM; ——, PFA. (a) $k_{99}/D = 0.05$; (b) $k_{99}/D = 0.12$; (c) $k_{99}/D = 0.15$.

particular, values and locations of mean radial velocity peaks are well estimated for a wide range of radial locations by the PFA resolved solution. It is customarily in the study of wall-jets to define an inner layer thickness as the wall-normal distance at which the radial velocity profile is maximum (Wu et al. (2016)). Similarly, an outer layer thickness is defined as the outermost wall-normal location where the radial velocity is half its maximum value at the same radial location. Inner and outer layer distributions along the radial direction are depicted in figure 5. For the $k_{99}/D = 0.05$ case, the agreement on the inner layer thickness between the PFA and IBM is good for $r/D < 3$, while the discrepancy becomes more evident for larger radial locations. From the figure it is also noted that the

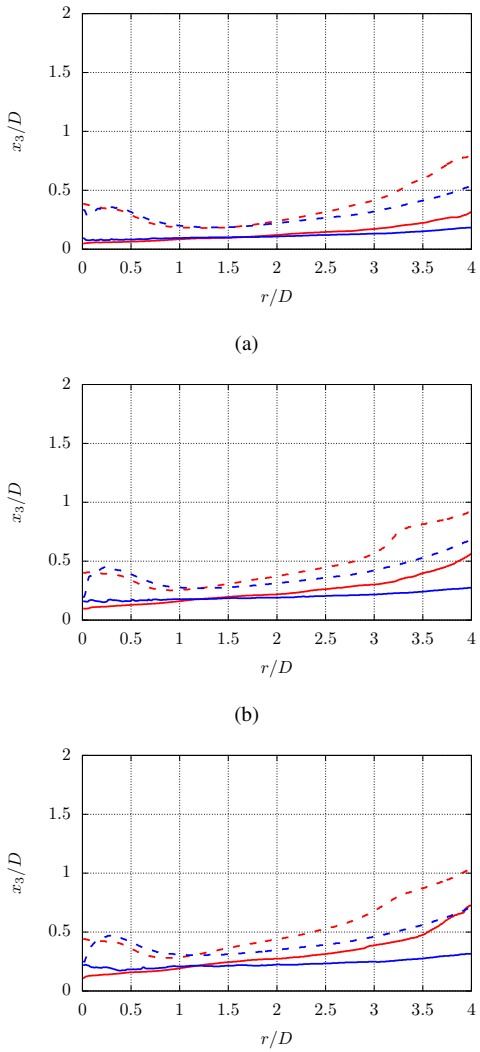

Figure 5: Inner and outer layer distributions along the impingement plate. ——, IBM inner layer; - - - -, IBM outer layer; ——, PFA inner layer; - - - -, PFA outer layer. (a) $k_{99}/D = 0.05$; (b) $k_{99}/D = 0.12$; (c) $k_{99}/D = 0.15$.

thickness of the outer layer is also well estimated by the PFA for the case with $k_{99}/D = 0.05$ for all radial locations $r/D < 2.5$. For the other two cases having a larger k_{99}, the estimation of the inner and outer layer thicknesses with the PFA is also reasonably good, but departures from the IBM resolved solution start already from smaller radial distances ($r/D > 2$ for both the inner and outer layer approximately).

One of the most important flow features affected by surface roughness is the total stress at the wall. When surface roughness is considered, the total wall-stress consists of the viscous stress and the pressure drag induced by roughness elements. Since both, the IBM and PFA methods adopted in this study employ a volume force distribution to introduce the effects of roughness, this force distribution can be used to estimate the total stress at the wall. The volume force introduced by either method is averaged, other than in time and circumferential direction, also in the wall normal direction. The resulting averaged force results in a distribution along the radial direction. The mean radial force distributions are depicted in figure 6 for all the three investigated rough surfaces. The scatter

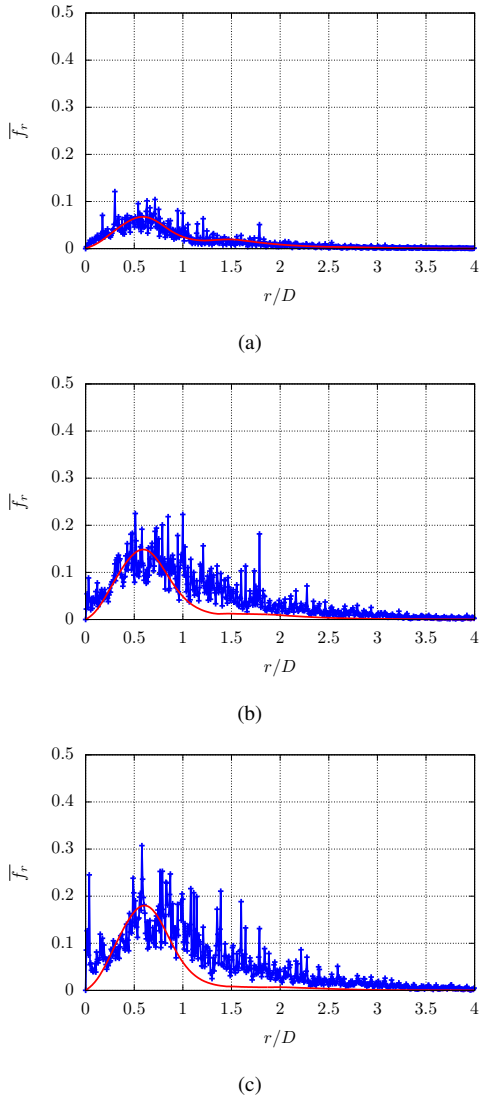

Figure 6: IBM and PFA averaged radial forcing distribution along the plate. ——, IBM; ——, PFA. (a) $k_{99}/D = 0.05$; (b) $k_{99}/D = 0.12$; (c) $k_{99}/D = 0.15$.

of the IBM radial forcing should be expected since the volume force distribution at different (x_1, x_2) locations the required forcing will greatly differ in both intensity and wall-normal height distribution. On the other hand, the PFA volume force is applied evenly at each wall-normal height x_3 and the averaging process leads in the end to a smooth curve. The case with the smallest roughness size (*i.e.* $k_{99}/D = 0.05$) displays the best agreement between the PFA and IBM radial forcing distributions. It is also emphasized that this is

the case that displays the best agreement for the mean velocity statistics. In the other two cases, the overall shape of the radial forcing distributions remains similar for both the PFA and IBM resolved solutions, even though the PFA estimated one decays faster with increasing radial distance. This symptom suggests that additional finer tuning is required for the two cases. In fact, it is recalled that all the three PFA resolved cases adopt the same model constants and the only difference lies in the different roughness shape function used to spread the volume forces in the wall-normal direction.

4 Conclusions

In this work, the PFA was used to introduce the effects of surface roughness on the mean velocity field statistics of a turbulent impinging jet. The examined flow configuration offers the chance to test the novel PFA (presented in Forooghi et al. (2018a)) in the context of spatially developing turbulent flows over rough surfaces. After the jet impingement, a wall-jet develops along the radial direction. To the authors knowledge, it is the first time that the PFA is applied to such type of non-equilibrium flows. To test the efficacy of the method, reference DNS using an IBM strategy to resolve the surface roughness were carried out during this study. The presented results show good agreement between the PFA and IBM resolved solutions for the mean velocity field and the radial distributions of the total wall stress. Such good correspondence is quite remarkable given that no particular tuning was applied beforehand to the PFA model constants but they were derived from a turbulent channel flow configuration. This proves the robustness of the approach and encourages future developments of the PFA. More precisely, it should be possible to fully characterize the model constants starting from the roughness topology. This was already suggested in the original version of the PFA presented in Busse and Sandham (2012). The resulting method would be completely determined by the roughness geometry alone, thus avoiding the burden of tuning any model constant. In addition, the introduction of a wall-normal component of the volume force might be beneficial for flow configurations, such as the impinging jet, where an intense wall-normal velocity component is expected.

Acknowledgments

Support by the German Research Foundation (DFG) under Collaborative Research Centre SFB/TRR150 (project number 237267381) is greatly acknowledged.
The simulations are performed on the national supercomputer HPE Apollo Hawk at the High Performance Computing Center Stuttgart (HLRS) under the grant number zzz44198

References

Busse, A. and Sandham, N. D. (2012), Parametric forcing approach to rough-wall turbulent channel flow, *J. Fluid Mech.*, vol. 712 p. 169–202.

Fisher, P. F., Lottes, J. W. and Kerkemeier, S. G. (2008-2020), NEK5000 v19.0., URL `https://nek5000.mcs.anl.gov/`, Argonne National Laboratory, Illinois.

Forooghi, P., Frohnapfel, B., Magagnato, F. and Busse, A. (2018a), A modified parametric forcing approach for modelling of roughness, *Int. J. of Heat and Fluid Flow*, vol. 71 pp. 200–209.

Forooghi, P., Weidenlener, A., Magagnato, F., Böhm, B., Kubach, H., Koch, T. and Frohnapfel, B. (2018b), DNS of momentum and heat transfer over rough surfaces based on realistic combustion chamber deposit geometries, *Int. J. of Heat and Fluid Flow*, vol. 69 pp. 83–94.

Goldstein, D., Handler, R. and Sirovich, L. (1993), Modeling a no-slip flow boundary with an external force field, *J. of Comp. Physics*, vol. 105 pp. 354–366.

Kaviany, M. (2012), *Principles of heat transfer in porous media*, Springer Science & Business Media.

Maday, Y. and Patera, A. (1989), Spectral element methods for the incompressible Navier-Stokes equations, in *State of the art surveys on computational mechanics ASME*, pp. 71–143.

Napoli, E., Armenio, V. and De Marchis, M. (2008), The effect of the slope of irregularly distributed roughness elements on turbulent wall-bounded flows, *J. Fluid Mech.*, vol. 613 p. 385–394.

Pèrez-Ràfols, F. and Almqvist, A. (2019), Generating randomly rough surfaces with given height probability distribution and power spectrum, *Tribology Int.*, vol. 131 pp. 591–604.

Vafai, K. and Kim, S. J. (1995), On the limitations of the brinkman-forchheimer-extended darcy equation, *Int. J. of Heat and Fluid Flow*, vol. 16 pp. 11–15.

Wu, W., Banyassady, R. and Piomelli, U. (2016), Large-eddy simulation of impinging jets on smooth and rough surfaces, *J. of Turbulence*, vol. 17 pp. 847–869.